Check for updates

Sensors

How to cite: *Angew. Chem. Int. Ed.* **2021**, *60*, 6488–6495
International Edition: doi.org/10.1002/anie.202011983
German Edition: doi.org/10.1002/ange.202011983

Spatiotemporal Measurement of Osmotic Pressures by FRET Imaging

Wenbo Zhang, Luca Bertinetti, Kerstin G. Blank, Rumiana Dimova, Changyou Gao, Emanuel Schneck, and Peter Fratzl**

Abstract: *Osmotic pressures (OPs) play essential roles in biological processes and numerous technological applications. However, the measurement of OP in situ with spatiotemporal resolution has not been achieved so far. Herein, we introduce a novel kind of OP sensor based on liposomes loaded with water-soluble fluorescent dyes exhibiting resonance energy transfer (FRET). The liposomes experience volume changes in response to OP due to water outflux. The FRET efficiency depends on the average distance between the entrapped dyes and thus provides a direct measure of the OP surrounding each liposome. The sensors exhibit high sensitivity to OP in the biologically relevant range of 0–0.3 MPa in aqueous solutions of salt, small organic molecules, and macromolecules. With the help of FRET microscopy, we demonstrate the feasibility of spatiotemporal OP imaging, which can be a promising new tool to investigate phenomena involving OPs and their dynamics in biology and technology.*

Introduction

The conversion of chemical into mechanical energy is an essential function in all living systems as well as in many technical processes. Molecular motors are essential components of cells that generate force by burning ATP, the cell-internal fuel. Within our muscles, molecular motors are responsible for animal locomotion, but they also mediate cell motility and adhesion and many other cellular processes. In plants, force generation and organ movement is often linked to turgor pressure, which is generated by another type of chemo-mechanical conversion based on osmotic gradients. These are known for more than hundred years[1] to be critical for a variety of cell functions,[2] living tissue organizations[3] and vital activities.[4] Osmotic pressure is recognized as an important biophysical cue as it can induce cell volume changes, which in turn activate osmoregulatory responses[4] and can determine, for example, stem cell fate.[5] Moreover, osmotic gradients are exploited by bacteria to promote spreading of colonies and to outcompete the growth of other cells.[6] In many cases, osmotic pressure is regulated for mechanical purposes: plants are well known to use osmotic pressure to create turgor for cell expansion and organ movements, such as the opening of a flower.[7] Another example is cartilage, which is stabilized by the swelling pressure of proteoglycans counter-balanced by the tension of (type II) collagen.[3,8] For example, in intact joints, there is a gentle grading of fixed charge density of cartilage and hence of osmotic pressure from the articular surface to the deep zone.[3,9] In addition, static and dynamic osmotic pressure gradients also occur in many other contexts from soil sciences,[10] to colloidal sciences,[11] water treatment,[12] energy generation,[13] material engineering,[14] and membrane filtration.[15]

In contrast to molecular motors, the functions of which have been studied in great detail,[16] much less is known about the potential roles of osmotic pressures, especially in animal tissues. One of the reasons is the lack of in situ probes for osmotic strength sensing. Such sensors would not only be important in biological contexts but also in all situations where osmotic processes need to be monitored in-operando from biology to physical chemistry and to engineering. The goal of the present work is to develop a local probe for spatiotemporal monitoring of osmotic stresses through light microscopy.

At present, the osmotic strength of homogeneous solutions is usually determined by measuring and analyzing colligative properties of the solutions, such as freezing-

[*] Dr. W. Zhang, Dr. L. Bertinetti, Prof. P. Fratzl
Department of Biomaterials,
Max Planck Institute of Colloids and Interfaces
14476 Potsdam (Germany)
E-mail: Peter.Fratzl@mpikg.mpg.de

Dr. K. G. Blank
Mechano(bio)chemistry,
Max Planck Institute of Colloids and Interfaces
14476 Potsdam (Germany)

Dr. R. Dimova
Department of Theory & Bio-Systems,
Max Planck Institute of Colloids and Interfaces,
14476 Potsdam (Germany)

Prof. C. Gao
MOE Key Laboratory of Macromolecular Synthesis and Functionalization, Department of Polymer Science and Engineering, Zhejiang University, Hangzhou 310027 (China)

Prof. E. Schneck
Department of Biomaterials,
Max Planck Institute of Colloids and Interfaces
14476 Potsdam (Germany)
and
Department of Physics, Technische Universität Darmstadt
64289 Darmstadt (Germany)
E-mail: schneck@fkp.tu-darmstadt.de

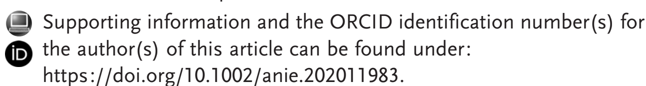

Supporting information and the ORCID identification number(s) for the author(s) of this article can be found under: https://doi.org/10.1002/anie.202011983.

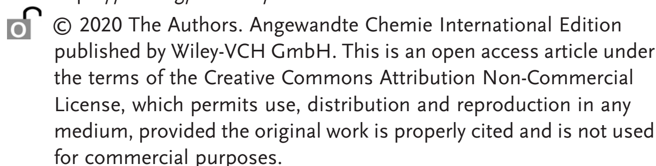

© 2020 The Authors. Angewandte Chemie International Edition published by Wiley-VCH GmbH. This is an open access article under the terms of the Creative Commons Attribution Non-Commercial License, which permits use, distribution and reproduction in any medium, provided the original work is properly cited and is not used for commercial purposes.

point[17] and vapor-pressure depression.[18] Alternatively, the osmotic pressure can be measured by a setup composed of manometers and semipermeable membranes.[19] However, these conventional methods have no spatial resolution and are therefore inapplicable to measurements of osmotic pressures in situ or in vivo. Therefore, a method for the spatiotemporal measurement of the osmotic pressure remains highly desirable.

Phospholipid liposomes exhibit permeability properties similar to those of biological membranes,[20] which constitute semi-permeable barriers capable of creating and maintaining defined osmotic pressures required for cellular activities.[21] On timescales of seconds to hours, liposomes are water-permeable but vastly impermeable to ions, macromolecules, and most water-soluble molecules. Compared with semi-permeable polymer microcapsules[22] and polymer membranes (polymersomes),[23] liposomes are highly deformable due to the low bending rigidity of lipid bilayers,[24] especially when composed of lipids with un-saturated alkyl chains.[25] In fact, various studies have demonstrated the response of liposomes to external osmotic pressures in terms of volume and shape changes.[17,25,26] With that, liposomes lend themselves towards their application as sensitive osmotic pressure sensors.

FRET (Förster resonance energy transfer), the nonradiative transfer of excitation energy from an excited donor dye to a proximal ground-state acceptor dye,[27] has been employed to design various fluorescence-based sensors.[28] FRET occurs when donor and acceptor dyes are in nanometric proximity, in which case the donor fluorescence emission is decreased, and the acceptor emission is increased (sensitized emission). The method is ratiometric and thus eliminates ambiguities due to the measurement geometry, the probe concentration, etc., by self-calibration of two emission bands.[28a,29] Donors and acceptors that are covalently linked, free in solution, or contained in restricted geometries, have been used to study macromolecule structures, interactions, and crowding, and to detect analytes or hydrogel deformation, etc.[30] For free dyes in solution, diffusion significantly enhances the energy transfer efficiency, such that considerable FRET is observed even for comparatively low dye concentrations.[31] By combining FRET with optical microscopy it is possible to obtain quantitative spatiotemporal information on intra- and intermolecular distances.[29c,32] In fact, ratiometric FRET sensors have previously been used to quantify macromolecular crowding in living cells,[33] an aspect that is related to osmotic pressure effects.

Here, we introduce FRET-based sensors for the direct quantification of osmotic pressures (Figure 1a). They are based on liposomes loaded with two highly water-soluble FRET dyes, ATTO 488 and ATTO 542. POPC (1-palmitoyl-2-oleoyl-glycero-3-phosphocholine), a typical naturally-occurring monounsaturated phospholipid forming liquid-crystalline bilayers at all relevant temperatures,[34] was chosen as

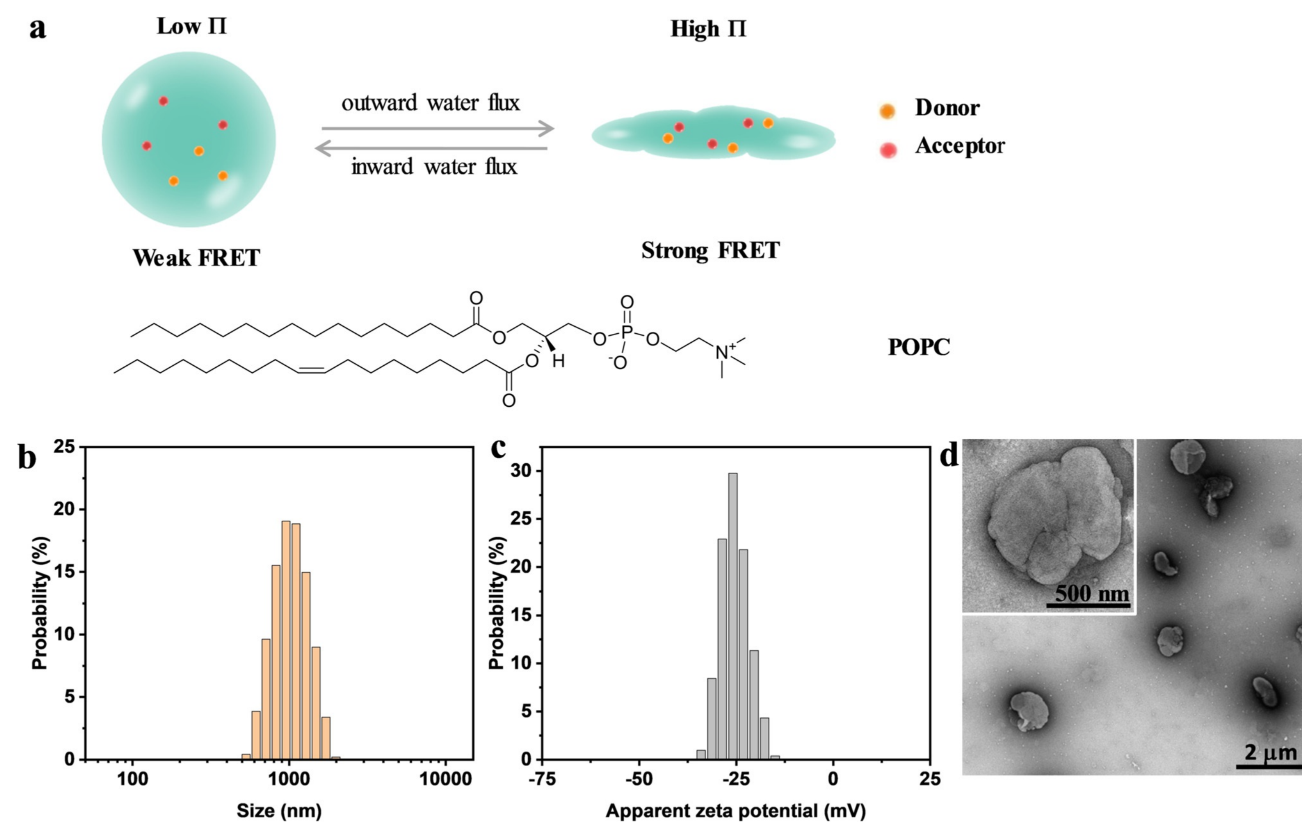

Figure 1. Osmotic pressure sensors based on dye-loaded liposomes (POPC-D-A). a) Schematic illustration of the working principle: The osmotic pressure Π leads to liposome shrinkage and thus to closer donor–acceptor proximity, enhancing FRET. b,c) Distributions of size (b) and zeta potential (c) of POPC-D-A liposomes in water as obtained by dynamic light scattering (DLS) and phase analysis light scattering (PALS), respectively. d) TEM images of POPC-D-A liposomes in dry state (inset, higher magnification) stained with 1% uranyl acetate.

the constituent of the semipermeable liposome membrane. The intra-liposomal dye concentration was chosen to be 50 μM. The associated sensor-inherent osmotic pressure (≲ 1 kPa) is negligible compared to the external osmotic pressures investigated. The sensitivity and applicable pressure range of the sensors depend on two specific features. The first one is the liposomes' relative volume change upon exposure to osmotic pressure Π, determined by the liposome size as well as the bending and stretching elastic properties of the constituting lipid bilayers. The second one is the response of the FRET efficiency, measured in the form of the (sensitized acceptor emission)/(donor emission) ratio R, to the resulting intra-liposomal dye concentration changes. Both features taken together can be conveniently mapped onto a "R versus Π"-calibration curve based on which the osmotic pressure at a sensor's position in an unknown environment is obtained from a simple measurement of the FRET efficiency. Combined with FRET microscopy, this procedure enables spatiotemporal osmotic pressure imaging.

Results and Discussion

Dye-loaded liposomes were prepared by a simple extrusion method (Figure S1). Dry POPC thin films on the inner walls of a glass vial were first hydrated with a mixed aqueous solution of ATTO 488 (donor) and ATTO 542 (acceptor) dyes, resulting in multilamellar aggregates. Liposomes containing the donor ("D") and acceptor ("A") dyes, termed "POPC-D-A" in the following, were then obtained by extrusion (see SI) and removal of extra-liposomal free dyes was achieved via rinsing and centrifugation. The average hydrodynamic diameter in water, as measured by dynamic light scattering (DLS) was ≈1 μm (Figure 1b). The zeta potential (Figure 1c) was found to be ≈−25 mV, similar to that of POPC liposomes without dye loading (Figure S2) and consistent with earlier reports.[35] Transmission electron microscopy (TEM) images show that some POPC-D-A liposomes are multi-lamellar and multi-compartmented (Figure 1d); however the morphology may change upon drying.

ATTO 488 (MW = 804 g mol^{-1}) and ATTO 542 (MW = 1028 g mol^{-1}) were chosen as the donor and acceptor fluorophores, respectively, because of their excellent water solubility, high fluorescence quantum yield and high photostability,[36] as well as negligible interaction with zwitterionic lipid bilayers.[37] Moreover, the fluorescence spectrum of ATTO 488 and the absorption spectrum of ATTO 542 in water show considerable overlap (Figure 2a), which is a prerequisite for FRET.[38] The strong dependence of the FRET efficiency on the distance between donors and acceptors[38] (as the inverse sixth power of the distance) constitutes the basis for the utility of this phenomenon in sensing. In an aqueous solution of FRET pair dyes at a fixed stoichiometry, the donor-acceptor distances are relevant with the dye concentration. To study the sensitivity of the FRET efficiency between ATTO 488 and ATTO 542 to volume (i.e. distance) changes, the fluorescence spectra of aqueous ATTO 488, ATTO 542 and 1:1 mixed solutions were measured for a series

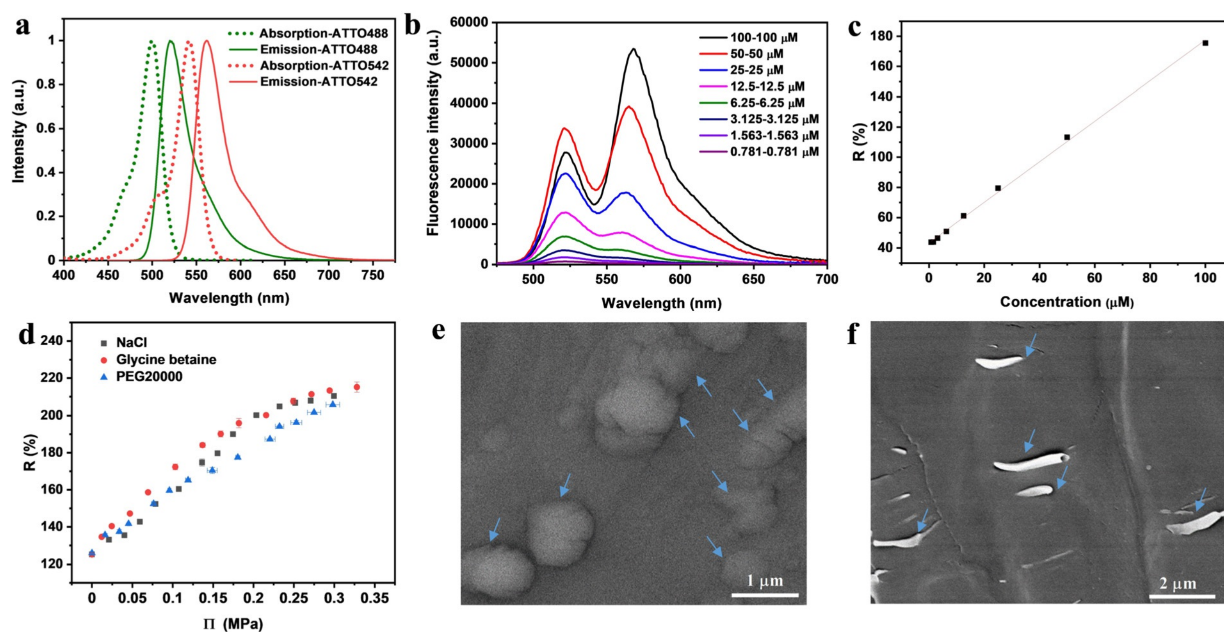

Figure 2. Sensing of osmotic pressures. a) Normalized UV/Vis absorption spectra and fluorescence emission spectra of ATTO 488 (donor) and ATTO 542 (acceptor) dyes in water. b) Fluorescence emission spectra of ATTO 488—ATTO 542 mixture (1:1 molar ratio) in water with different concentrations (0.781–100 μM) at a fixed excitation wavelength of 440 nm. c) Emission ratio R as a function of the dye concentration in a 1:1 molar ratio in bulk aqueous solution. The solid line is a linear fit to the data points (coefficient of determination = 0.998). d) R obtained with POPC-D-A liposomes loaded with a dye concentration of 50 μM (1:1 molar ratio) as a function of the external osmotic pressure generated by various concentrations of NaCl, GB, or PEG. The excitation wavelength was 440 nm. e,f) Cryo-SEM images of POPC-D-A liposomes in water (e) and NaCl solution (0.35 %, 0.27 MPa) (f). Blue arrows indicate individual POPC-D-A liposomes.

 © 2020 The Authors. Angewandte Chemie International Edition published by Wiley-VCH GmbH

of concentrations, using a fixed excitation wavelength of $\lambda = 440$ nm (Figure S3, Figure 2b).

In the fluorescence spectra of the mixtures, the contribution of the acceptor emission systematically increases relative to the donor emission with increasing concentration (Figure 2b). This observation clearly confirms the sensitized emission of the acceptor (ATTO 542). In order to quantify the FRET efficiency, the (sensitized acceptor emission)/(donor emission) ratio was used, defined here as the ratio between the emission intensities at 562 nm and 520 nm. In the following, this ratio is referred to as the emission ratio R. Figure 2c shows R as a function of the dye concentration in a 1:1 molar ratio, which is seen to increase monotonically with the concentration. In fact, in the investigated concentration range the increase is surprisingly linear. The solid line in Figure 2c is a linear fit (coefficient of determination = 0.998) with $R = 43.33 + 1.34c$, where c is the dye (donor/acceptor) molarity in μM. Excitation at 458 nm (Figure S4) gave similar results to those obtained with 440 nm excitation. Rough estimates of the average next neighbor distance between two dye molecules (assumed to behave as ideal solutes) and of the probability distribution of next neighbor distances confirms that donors and acceptors have a considerable probability to be relatively close to each other (< 10 nm), see Supporting Information. Moreover the fluorophore diffusion and the fluorophore size effect (the diameter of a typical dye chromophore is 10–15 Å) can be considered to further promote small donor-acceptor distances.[31] Possible interactions between the donor and the acceptor fluorophores, such as electrostatic attraction, can influence the donor-acceptor distance and thus the FRET efficiency.[31a] However, these effects are empirically captured by the calibration curves based on which the emission ratios are interpreted.

In the following studies, a fixed dye concentration of 50 μM (1:1 molar ratio) was used to prepare the dye-loaded POPC-D-A liposomes. To determine the osmotic response, sodium chloride (NaCl), the most abundant solute in extracellular fluid; glycine betaine (GB), a typical intracellular organic osmolyte able to stabilize proteins;[39] and polyethylene glycol (PEG, average MW = 20 000 g mol^{-1}), an inert macromolecule widely used in the control of osmotic pressures,[26a,40] were used. For each solute type, a series of solutions with independently measured osmotic pressures were prepared (Figure S5). The POPC-D-A liposomes were then exposed to the respective solutions and the FRET efficiency was determined from the recorded fluorescence spectra. Figure 2d shows R of the intra-liposomal dyes as a function of the osmotic pressure in the range of $0 \leq \Pi \leq 0.3$ MPa for all three solute types. At $\Pi = 0$, the emission ratio ($R \approx 125\,\%$) is similar to the one in a bulk solution of the same dyes at 50 μM ($R \approx 115\,\%$, see Figure 2c). This consistency indicates that the dyes partition approximately evenly inside and outside the liposomes during the preparation process and is in line with the ratiometric character of the FRET mechanism, which eliminates the influence of the sample geometry and of the overall amount of dye in a sample. The same consistency is observed when comparing liposomes loaded with 25 μM dyes ($R \approx 85\,\%$, see Figure S6) with a 25 μM bulk solution ($R \approx 80\,\%$, see Figure 2c). Molecular energy transfer in general can occur via radiative and non-radiative mechanisms.[41] In the present case the non-radiative mechanism FRET can be considered dominant based on the above results and similar reported cases.[31a,b,42]

Irrespective of the solute type, the emission ratio R increases monotonically with Π, first approximately linearly at low pressures ($\Pi \lesssim 0.2$ MPa) and then turning to a weaker pressure dependence at higher pressures ($\Pi > 0.2$ MPa). In view of the virtually linear concentration dependence of R in bulk (Figure 2c), this observation indicates that the volumetric response of the liposomes to the external osmotic pressure is non-linear. The liposomes are more easily deformed when in their initial spherical shape than when already partially deflated, a behavior that must be attributed to the bending rigidity of the lipid bilayer. The shape changes of the liposomes were observed with cryo scanning electron microscopy (cryo-SEM), which showed that the original liposomes are nearly spherical in pure water (Figure 2e, indicated with blue arrows) and flattened at high osmotic pressures (Figure 2f, indicated with blue arrows). The disk-like shapes observed here are qualitatively consistent with those experimentally observed and theoretically predicted earlier under the assumption of conserved bilayer surface area.[17,26b,43] Assuming that the fluorophores inside the liposomes behave as in a bulk dye solution, the relative volume change (i.e., water loss) can be estimated from the bulk dye concentration at which the same emission ratio is observed. For example, for POPC-D-A liposomes subject to $\Pi = 0.1$ MPa, where the emission ratio is $R \approx 160\,\%$ (see Figure 2d), the equivalent dye bulk concentration is $c_{\mathrm{equiv}} \approx 85$ μM (see Figure 2c). The associated volume reduction is then $1 - c_0/c_{\mathrm{equiv}} \approx 41\,\%$, where $c_0 = 50$ μM is the dye loading concentration. The average fluorophore distance can be roughly estimated within the Wigner-Seitz approximation. Further taking into account the effects of fluorophore diffusion, size and interactions, the FRET probabilities can be estimated, if desired, with the help of specific statistical methods such as Gösele's theory.[31c]

Importantly, the emission ratio at a given osmotic pressure is consistent among the three solute types (Figure 2c). Minor deviations between PEG on one side and the two other solute types on the other side must be attributed to systematic uncertainties in the determination of the osmotic pressure, which is measured in different ways for macromolecules and small solutes (see Supporting Information). This result demonstrates that the POPC-D-A liposomes are equally impermeable to all osmotic agents investigated and thus exhibit the same response to osmotic stress irrespective of its source. Repeated experiments with the same batch of liposomes demonstrated good reproducibility of the osmotic sensing under the same conditions (Figure S7). The reversibility of the osmotic response was confirmed in re-dilution experiments (see Figure S8).

Taken together, the results obtained are in line with the schematic illustration of the osmotic pressure sensing principle in Figure 1a: The liposomes shrink due to the osmotically driven outward flux of water through the lipid bilayer, such that the dye concentration in the liposome cavity increases, and in turn the FRET efficiency. In fact, adjusting the bilayer bending rigidity, the spectral overlap between the fluoro-

 © 2020 The Authors. Angewandte Chemie International Edition published by Wiley-VCH GmbH

phores chosen, the initial intra-liposomal dye concentration and loaded osmotically active solutes on the inside should allow producing sensors optimized for a wide range of osmotic pressures. For example, the osmotic pressure range can readily be extended towards physiological salt concentrations and beyond by loading liposomes with osmotically active solutes on the inside, as exemplarily shown for 0.1% NaCl (Figure S9). The increase in the range of accessible osmotic pressures comes, however, as a trade-off with sensitivity, as evidenced by the reduced slope of emission ratio versus osmotic pressure (Figure S9), which emphasizes the opportunity and the need for optimizing the sensors to the required pressure range.

With the sensing principle established, the possibility of spatiotemporal imaging of osmotic pressures with POPC-D-A liposomes was investigated. Confocal laser scanning microscopy (CLSM) was chosen for sensitized emission FRET imaging at an excitation wavelength of $\lambda = 458$ nm (see SI for the details). At high magnification (eyepiece 630 ×), well-dispersed individual liposomes can be observed exhibiting donor emission, sensitized acceptor emission, and direct acceptor emission signals (Figure 3a). In the next step, a drop of POPC-D-A liposome suspension placed on a glass slide was imaged at lower magnification by exciting the donor fluorophores and recording the emission from the donor (donor signal, Figure 3b upper left panel) and the acceptor fluorophores (sensitized acceptor emission signal, Figure 3b upper right panel) separately. The direct acceptor emission (Figure 3b lower left panel) was probed via selective acceptor excitation with a longer wavelength ($\lambda = 561$ nm). According to established procedures,[29d,32a,44] the FRET efficiency is then again measured in the form of the ratio R between the sensitized acceptor emission and the donor emission for each pixel (Figure 3b lower right panel). Figure 3c shows emission ratio images of POPC-D-A-loaded droplets of NaCl solutions with systematically increasing NaCl concentrations corresponding to osmotic pressures in the range between 0 and ≈ 0.31 MPa. The emission ratio, averaged in a region of interest indicated with a red rectangle, is seen to increase systematically with increasing osmotic pressure, from $R \approx 53\%$ (at $\Pi = 0$) to $R \approx 87\%$ (at $\Pi \approx 0.31$ MPa). Quantitative analysis yielded a calibration curve (Figure 3d), whose shape is consistent with the one obtained in the spectrofluorometer (Figure 2d). Note, however, that the R-values obtained from the fluorescence microscopy cannot be quantitatively compared with those obtained from the fluorescence spectroscopy due to different collection and calculation methods of the signal. The spatial resolution at which the osmotic pressure can be imaged is mainly related to the average distance between individual sensor-liposomes in the sample and can be improved by increasing the liposome concentration.

In order to illustrate the feasibility of in situ mapping of spatially distributed osmotic pressures, two droplets of aqueous POPC-D-A liposome suspensions, one containing pure water and one containing a NaCl solution of $\Pi = 0.285$ MPa, were first brought to proximity (see Figure 4a for the emission ratio image) and then brought to coalescence (Figure 4b). The spatially dependent distribution of emission ratio (R) values reveals the transient formation of an osmotic pressure gradient (indicated with the yellow arrow) across the contact zone. Moreover, regions of elevated osmotic pressures can be clearly identified along the edges of the solution (indicated with white arrows). They can be considered

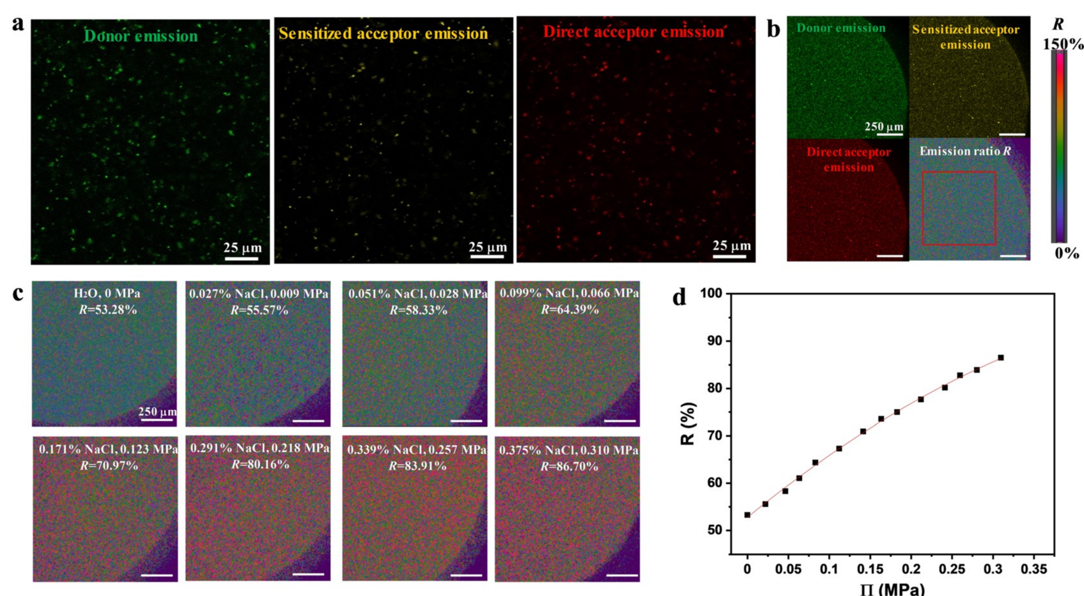

Figure 3. Application of POPC-D-A liposomes for osmotic pressure imaging. a) Confocal laser scanning microscopy (CLSM) images of individual POPC-D-A liposomes in water at high magnification, with the donor emission signal on the left (Ex 458 nm, Em 468–538 nm), the sensitized acceptor emission signal in the middle (Ex 458 nm, Em 571–700 nm), and the direct acceptor emission signal on the right (Ex 561 nm, Em 571–700 nm). b) CLSM images at lower magnification. The lower right image shows the emission ratio R in each pixel. c) Emission ratio (R) images of POPC-D-A liposomes in NaCl solutions of various osmotic pressures. d) Calibration curve recorded at various osmotic pressures. The solid line is an empirical second-order polynomial fit to the data points (coefficient of determination = 0.998).

 © 2020 The Authors. Angewandte Chemie International Edition published by Wiley-VCH GmbH

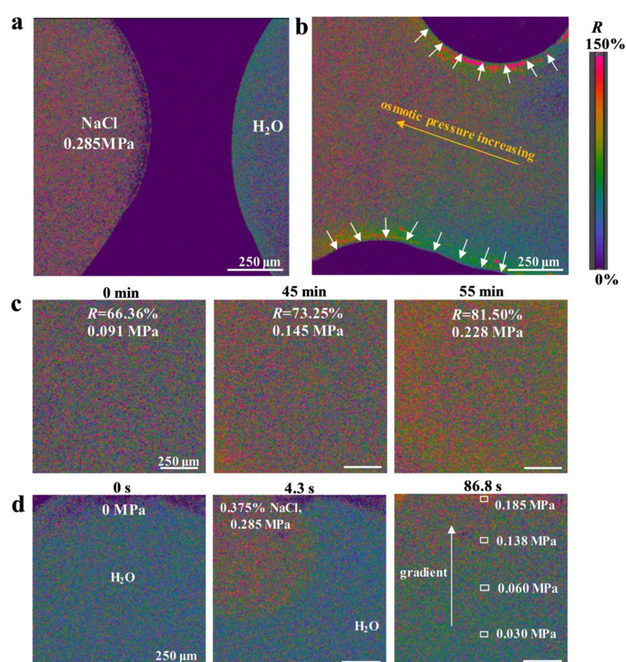

Figure 4. FRET imaging for the in situ spatiotemporal measurement of osmotic pressures. a) Emission ratio (R) image of two droplets of aqueous POPC-D-A liposome suspensions with different osmotic pressures. They exhibit clearly different FRET efficiencies. b) Emission ratio (R) image after droplet coalescence exhibiting distinct osmotic pressure gradients. c) Monitoring of osmotic pressure changes of a NaCl solution during evaporation process. d) Spatiotemporal imaging of an osmotic-pressure gradient generated through localized coalescence of a water drop and a drop of NaCl solution. The indicated osmotic pressures are calculated using the calibration curve (Figure 3 d).

manifestations of steep osmotic pressure gradients due to water evaporation under steady-state conditions.

In the next step, the in situ spatiotemporal measurement of osmotic pressures by time-lapse fluorescence imaging and subsequent quantitative analysis was further explored. To this end, the liposomes were used for real-time in situ monitoring of dynamically changing osmotic pressures during an evaporation process of NaCl solution. A drop of NaCl solution of moderate osmotic pressure ($\Pi \approx 0.095$ MPa) containing POPC-D-A liposomes was placed on the glass bottom of a 20-mm dish with lid and let evaporate. Time-lapse fluorescence imaging shows that the emission ratio R increased gradually over time within 1 h (Figure 4c, Figure S10). With the calibration curve (Figure 3 d) at hand, the osmotic pressures were calculated and are indicated in Figure 4c. The solution concentrations (Table S1) were further calculated according to the osmotic pressure-mass fraction calibration curve (Figure S5d), where osmotic pressure and NaCl concentration were seen to increase monotonically with time. These results clearly demonstrate that the POPC-D-A liposome sensors can be used to measure dynamically changing osmotic pressures in situ. A possible disturbance of the liposome distribution in the droplets due to coffee-ring effect and Marangoni flow does not affect the measurement of osmotic pressures as a result of the ratiometric character of FRET microscopy. Similar sensors may in fact be used to gain further insights into these two phenomena.

In a continuous solution with an initial osmotic pressure gradient, the osmotic pressure distribution exhibits spatiotemporal evolution until an equilibrium is reached via solvent and solute diffusion. As shown in Figure 4 d, this process, too, can be monitored by using the POPC-D-A liposome sensors. With a self-made device (Figure S11), an initially steep osmotic pressure gradient was generated through localized coalescence of a water drop and a drop of NaCl solution ($\Pi \approx 0.285$ MPa, concentration of 0.375 %), both containing POPC-D-A liposomes. Time-lapse emission ratio (R) imaging enabled monitoring the evolution of the osmotic pressure distribution and of the equilibration process (Figure 4 d, Figure S12 a–c). At each point in space the instantaneous osmotic pressure can be calculated according to the calibration curve (Figure 3 d). This was done exemplarily inside the four rectangles indicated in Figure 4 d (image on the right, recorded after 86.8 s). The obtained osmotic pressures for these four points along the osmotic gradient and over a distance of about 1 mm are 0.185, 0.138, 0.060, and 0.030 MPa, respectively, corresponding to NaCl concentrations of 0.249 %, 0.189 %, 0.092 %, and 0.053 %, respectively (Table S2). Spatially more highly resolved osmotic pressure and concentration data are reported in Figure S12 d and Table S2. The steepness of the osmotic pressure gradient was found to decrease gradually with time until a constant osmotic pressure was reached after $\approx$30 min (Figure S12).

The spatiotemporal evolution of the FRET efficiency is in principle governed not only by the spatiotemporal evolution of the osmotic pressure, but also by the temporal response of the liposomes to osmotic pressure changes. In order to estimate the role of the latter, the temporal response of the emission ratio R was determined in “pressure-jump experiments”, where the liposomes were added to homogeneous solutions of defined osmotic pressures, followed by rapid FRET measurements. As shown in Figure S13, the equilibrium value of R is already reached when the first FRET measurement was finished after 2 s. This finding is consistent with the reported virtually “immediate” osmotic response of 1,2-dioleoyl-sn-glycero-3-phosphocholine (DOPC) liposomes[17] and suggests that the spatiotemporal evolution of the FRET efficiency indeed reflects primarily the spatiotemporal evolution of the osmotic pressure. Moreover, the time-dependent measurements also show that the emission ratio does not change within the time frame of 1 h (Figure S13), demonstrating that photobleaching does not visibly affect the data obtained under our experimental conditions.

Conclusion

In summary, we have developed an osmotic pressure sensor based on FRET donor-acceptor loaded liposomes, which can be prepared with a simple method. It exhibits quick response and high sensitivity in measuring aqueous solutions of salt, small organic molecule, and polymer solutes. Taking advantage of fluorescence imaging, in situ spatiotemporal imaging of osmotic pressure is possible with these sensors.

 © 2020 The Authors. Angewandte Chemie International Edition published by Wiley-VCH GmbH

This can open a path from physical chemistry to biology where osmotic gradients play an important role. This work provides a proof-of-concept for in situ measurements of osmotic pressure in dynamic systems. Further investigations on its applications in life science will be the next step.

Acknowledgements

We thank Reinhild Dünnebacke, Carmen Remde, Andreas Fulterer from Leica company, Martina Delbianco, Giulio Fittolani and Heike Runge for their technical support in fluorescence spectroscopy, confocal microscopy, osmometry and electron microscopy. Financial support by the Max Planck Society and by the German Research Foundation via Emmy-Noether grant (SCHN 1396/1) is gratefully acknowledged. Open access funding enabled and organized by Projekt DEAL.

Conflict of interest

The authors declare no conflict of interest.

Keywords: fluorescence microscopy · FRET · imaging agents · liposomes · semi-permeable membranes

[1] W. R. G. Atkins, *Sci. Prog.* **1917**, *11*, 562 – 577.
[2] S. Tokuda, A. S. L. Yu, *Int. J. Mol. Sci.* **2019**, *20*, 3513.
[3] a) E. Han, S. S. Chen, S. M. Klisch, R. L. Sah, *Biophys. J.* **2011**, *101*, 916 – 924; b) S. R. Inamdar, E. Barbieri, N. J. Terrill, M. M. Knight, H. S. Gupta, *Acta Biomater.* **2019**, *97*, 437 – 450.
[4] M. B. Burg, J. D. Ferraris, *J. Biol. Chem.* **2008**, *283*, 7309 – 7313.
[5] M. Guo, A. F. Pegoraro, A. Mao, E. H. Zhou, P. R. Arany, Y. Han, D. T. Burnette, M. H. Jensen, K. E. Kasza, J. R. Moore, F. C. Mackintosh, J. J. Fredberg, D. J. Mooney, J. Lippincott-Schwartz, D. A. Weitz, *Proc. Natl. Acad. Sci. USA* **2017**, *114*, E8618 – E8627.
[6] a) J. Yan, C. D. Nadell, H. A. Stone, N. S. Wingreen, B. L. Bassler, *Nat. Commun.* **2017**, *8*, 327; b) A. Seminara, T. E. Angelini, J. N. Wilking, H. Vlamakis, S. Ebrahim, R. Kolter, D. A. Weitz, M. P. Brenner, *Proc. Natl. Acad. Sci. USA* **2012**, *109*, 1116 – 1121.
[7] L. Beauzamy, N. Nakayama, A. Boudaoud, *Ann. Bot.* **2014**, *114*, 1517 – 1533.
[8] a) A. Maroudas, *Nature* **1976**, *260*, 808 – 809; b) A. Maroudas, *Biophys. J.* **1968**, *8*, 575 – 595; c) A. Maroudas, E. Wachtel, G. Grushko, E. P. Katz, P. Weinberg, *Biochim. Biophys. Acta* **1991**, *1073*, 285 – 294.
[9] A. Maroudas, C. Bannon, *Biorheology* **1981**, *18*, 619 – 632.
[10] H. G. Jones, *J. Exp. Bot.* **2007**, *58*, 119 – 130.
[11] D. Carrière, M. Page, M. Dubois, T. Zemb, H. Cölfen, A. Meister, L. Belloni, M. Schönhoff, H. Möhwald, *Colloids Surf. A* **2007**, *303*, 137 – 143.
[12] K. Lutchmiah, A. R. D. Verliefde, K. Roest, L. C. Rietveld, E. R. Cornelissen, *Water Res.* **2014**, *58*, 179 – 197.
[13] M. Macha, S. Marion, V. V. R. Nandigana, A. Radenovic, *Nat. Rev. Mater.* **2019**, *4*, 588 – 605.
[14] a) M. Ballauff, *Prog. Polym. Sci.* **2007**, *32*, 1135 – 1151; b) C. M. Chen, S. Yang, *Polym. Int.* **2012**, *61*, 1041 – 1047.
[15] J. C. Chen, Q. L. Li, M. Elimelech, *Adv. Colloid Interface Sci.* **2004**, *107*, 83 – 108.
[16] a) E. R. Kay, D. A. Leigh, F. Zerbetto, *Angew. Chem. Int. Ed.* **2007**, *46*, 72 – 191; *Angew. Chem.* **2007**, *119*, 72 – 196; b) G. Saper, H. Hess, *Chem. Rev.* **2020**, *120*, 288 – 309.
[17] J. Pencer, G. F. White, F. R. Hallett, *Biophys. J.* **2001**, *81*, 2716 – 2728.
[18] a) H. G. Applegate, *Nature* **1960**, *186*, 232 – 233; b) N. P. Money, *Plant Physiol.* **1989**, *91*, 766 – 769.
[19] a) H. Vink, *Eur. Polym. J.* **1974**, *10*, 149 – 156; b) C. Nagesh, R. P. Paily, *J. Micromech. Microeng.* **2015**, *25*, 040519.
[20] B. L. S. Mui, P. R. Cullis, E. A. Evans, T. D. Madden, *Biophys. J.* **1993**, *64*, 443 – 453.
[21] P. K. J. Kinnunen, *Cell. Physiol. Biochem.* **2000**, *10*, 243 – 250.
[22] S. H. Kim, T. Y. Lee, S. S. Lee, *Small* **2014**, *10*, 1155 – 1162.
[23] E. Rideau, R. Dimova, P. Schwille, F. R. Wurm, K. Landfester, *Chem. Soc. Rev.* **2018**, *47*, 8572 – 8610.
[24] R. Dimova, *Adv. Colloid Interface Sci.* **2014**, *208*, 225 – 234.
[25] S. Emami, W. C. Su, S. Purushothaman, V. N. Ngassam, A. N. Parikh, *Biophys. J.* **2018**, *115*, 1942 – 1955.
[26] a) W. C. Su, D. L. Gettel, M. Chabanon, P. Rangamani, A. N. Parikh, *J. Am. Chem. Soc.* **2018**, *140*, 691 – 699; b) B. Lerebours, E. Wehrli, H. Hauser, *Biochim. Biophys. Acta Biomembr.* **1993**, *1152*, 49 – 60; c) S. U. A. Shibly, C. Ghatak, M. A. S. Karal, M. Moniruzzaman, M. Yamazaki, *Biophys. J.* **2016**, *111*, 2190 – 2201; d) E. Boroske, M. Elwenspoek, W. Helfrich, *Biophys. J.* **1981**, *34*, 95 – 109; e) J. Steinkuhler, R. L. Knorr, Z. Zhao, T. Bhatia, S. M. Bartelt, S. Wegner, R. Dimova, R. Lipowsky, *Nat. Commun.* **2020**, *11*, 905.
[27] a) I. L. Medintz, T. Pons, K. Susumu, K. Boeneman, A. M. Dennis, D. Farrell, J. R. Deschamps, J. S. Melinger, G. Bao, H. Mattoussi, *J. Phys. Chem. C* **2009**, *113*, 18552 – 18561; b) S. Z. Wu, Y. L. Luo, F. Zeng, J. Chen, Y. N. Chen, Z. Tong, *Angew. Chem. Int. Ed.* **2007**, *46*, 7015 – 7018; *Angew. Chem.* **2007**, *119*, 7145 – 7148.
[28] a) X. L. Zhang, Y. Xiao, X. H. Qian, *Angew. Chem. Int. Ed.* **2008**, *47*, 8025 – 8029; *Angew. Chem.* **2008**, *120*, 8145 – 8149; b) T. Pons, I. L. Medintz, K. E. Sapsford, S. Higashiya, A. F. Grimes, D. S. English, H. Mattoussi, *Nano Lett.* **2007**, *7*, 3157 – 3164; c) S. Preus, L. M. Wilhelmsson, *ChemBioChem* **2012**, *13*, 1990 – 2001.
[29] a) D. Srikun, E. W. Miller, D. W. Dornaille, C. J. Chang, *J. Am. Chem. Soc.* **2008**, *130*, 4596 – 4597; b) C. Ma, F. Zeng, L. F. Huang, S. Z. Wu, *J. Phys. Chem. B* **2011**, *115*, 874 – 882; c) S. R. Adams, A. T. Harootunian, Y. J. Buechler, S. S. Taylor, R. Y. Tsien, *Nature* **1991**, *349*, 694 – 697; d) A. Miyawaki, J. Llopis, R. Heim, J. M. McCaffery, J. A. Adams, M. Ikura, R. Y. Tsien, *Nature* **1997**, *388*, 882 – 887.
[30] a) Y. Y. He, Y. Nie, G. Cheng, L. Xie, Y. Q. Shen, Z. W. Gu, *Adv. Mater.* **2014**, *26*, 1534 – 1540; b) S. W. A. Reulen, M. Merkx, *Bioconjugate Chem.* **2010**, *21*, 860 – 866; c) I. L. Medintz, A. R. Clapp, H. Mattoussi, E. R. Goldman, B. Fisher, J. M. Mauro, *Nat. Mater.* **2003**, *2*, 630 – 638; d) J. Saha, A. D. Roy, D. Dey, S. Chakraborty, D. Bhattacharjee, P. K. Paul, S. A. Hussain, *Spectrochim. Acta Part A* **2015**, *149*, 143 – 149; e) T. Ng, A. Squire, G. Hansra, F. Bornancin, C. Prevostel, A. Hanby, W. Harris, D. Barnes, S. Schmidt, H. Mellor, P. I. H. Bastiaens, P. J. Parker, *Science* **1999**, *283*, 2085 – 2089; f) J. W. Neubauer, N. Hauck, M. J. Mannel, M. Seuss, A. Fery, J. Thiele, *ACS Appl. Mater. Interfaces* **2019**, *11*, 26307 – 26313.
[31] a) J. Saha, A. D. Roya, D. Dey, J. Nath, D. Bhattacharjee, S. A. Hussain, *Sens. Actuators B* **2017**, *241*, 1014 – 1023; b) S. Belušáková, V. Martínez-Martínez, I. L. Arbeloa, J. Bujdák, *J. Phys. Chem. C* **2017**, *121*, 8300 – 8309; c) U. Gösele, M. Hauser, U. K. A. Klein, R. Frey, *Chem. Phys. Lett.* **1975**, *34*, 519 – 522; d) A. Muratsugu, J. Watanabe, S. Kinoshita, *J. Chem. Phys.* **2014**, *140*, 214508.
[32] a) J. van Rheenen, M. Langeslag, K. Jalink, *Biophys. J.* **2004**, *86*, 2517 – 2529; b) G. W. Gordon, G. Berry, X. H. Liang, B. Levine, B. Herman, *Biophys. J.* **1998**, *74*, 2702 – 2713; c) A. Honda, S. R.

 © 2020 The Authors. Angewandte Chemie International Edition published by Wiley-VCH GmbH

Adams, C. L. Sawyer, V. Lev-Ram, R. Y. Tsien, W. R. G. Dostmann, *Proc. Natl. Acad. Sci. USA* **2001**, *98*, 2437 – 2442.
[33] a) A. J. Boersma, I. S. Zuhorn, B. Poolman, *Nat. Methods* **2015**, *12*, 227 – 229; b) D. Gnutt, M. Gao, O. Brylski, M. Heyden, S. Ebbinghaus, *Angew. Chem. Int. Ed.* **2015**, *54*, 2548 – 2551; *Angew. Chem.* **2015**, *127*, 2578 – 2581.
[34] a) B. J. Litman, E. N. Lewis, I. W. Levin, *Biochemistry* **1991**, *30*, 313 – 319; b) S. Leekumjorn, A. K. Sum, *J. Phys. Chem. B* **2007**, *111*, 6026 – 6033.
[35] A. Laouini, C. Charcosset, H. Fessi, R. G. Holdich, G. T. Vladisavljevic, *RSC Adv.* **2013**, *3*, 4985 – 4994.
[36] G. T. Dempsey, J. C. Vaughan, K. H. Chen, M. Bates, X. W. Zhuang, *Nat. Methods* **2011**, *8*, 1027 – 1036.
[37] Z. F. Zhang, D. Yomo, C. Gradinaru, *Biochim. Biophys. Acta Biomembr.* **2017**, *1859*, 1242 – 1253.
[38] a) B. Valeur, M. N. Berberan-Santos, *Molecular Fluorescence : principles and applications*, Wiley-VCH, Weinheim, **2013**; b) J. R. Lakowicz, *Principles of Fluorescence Spectroscopy*, Springer, New York, **2013**.
[39] a) P. H. Yancey, M. E. Clark, S. C. Hand, R. D. Bowlus, G. N. Somero, *Science* **1982**, *217*, 1214 – 1222; b) E. Schneck, D. Horinek, R. R. Netz, *J. Phys. Chem. B* **2013**, *117*, 8310 – 8321.
[40] J. Lagerwerff, H. E. Eagle, G. Ogata, *Science* **1961**, *133*, 1486 – 1487.
[41] D. L. Andrews, *Chem. Phys.* **1989**, *135*, 195 – 201.
[42] P. D. Sahare, V. K. Sharma, D. Mohan, A. A. Rupasov, *Spectrochim. Acta Part A* **2008**, *69*, 1257 – 1264.
[43] a) R. Lipowsky, *Nature* **1991**, *349*, 475 – 481; b) M. S. Long, C. D. Jones, M. R. Helfrich, L. K. Mangeney-Slavin, C. D. Keating, *Proc. Natl. Acad. Sci. USA* **2005**, *102*, 5920 – 5925.
[44] C. Berney, G. Danuser, *Biophys. J.* **2003**, *84*, 3992 – 4010.

Manuscript received: September 2, 2020
Revised manuscript received: November 6, 2020
Accepted manuscript online: November 14, 2020
Version of record online: February 3, 2021

 © 2020 The Authors. Angewandte Chemie International Edition published by Wiley-VCH GmbH